Seasonal Variations of the 40–50-Day Oscillation in Atmospheric Angular Momentum

DAVID S. GUTZLER

Atmospheric and Environmental Research, Inc., Cambridge, Massachusetts

ROLAND A. MADDEN

*National Center for Atmospheric Research, Boulder, Colorado**

(Manuscript received 14 November 1991, in final form 12 May 1992)

ABSTRACT

Seasonally varying spectral and cross-spectral calculations are carried out on multiyear time series of vertically and zonally averaged daily zonal wind fields to describe the seasonal cycle of the 40–50-day oscillation of atmospheric angular momentum. Intraseasonal variability (including 40–50-day fluctuations) of global momentum is largest in late boreal winter and smallest in boreal autumn; however, the 40–50-day spectral peak is most pronounced in boreal summer when lower-frequency intraseasonal variance is depressed. The 40–50-day spectral peak in global momentum is much less pronounced and apparently is restricted to a narrower frequency band, than corresponding peaks in zonal wind spectra from individual tropical rawinsonde stations. Contributions to global momentum fluctuations from three near-equal-area latitude bands (tropics, Northern Hemisphere, and Southern Hemisphere) are compared, confirming that intraseasonal momentum fluctuations are tropical in origin. The variance of extratropical momentum at this time scale is about an order of magnitude less than the tropical momentum variability. Coherent tropical–extratropical interactions are found principally in boreal winter, with the highest coherence between the tropics and Northern Hemisphere. The corresponding phase difference between tropical and Northern Hemisphere momentum is suggestive of poleward propagation of momentum out of the tropics.

1. Introduction

A 40–50-day spectral peak is observed in time series of zonal winds at individual tropical rawinsonde stations (Madden and Julian 1971) and in coupled fluctuations of the angular momentum of the atmosphere and solid earth (Anderson and Rosen 1983; Rosen and Salstein 1983). Preliminary conjectures that the oscillations in tropical wind and global momentum are related have been largely substantiated, although the dynamical link between the local variability (which projects principally onto zonal wavenumbers 1 and 2; Madden and Julian 1972) and the zonally averaged atmospheric momentum fluctuations has not been firmly established. Anderson and Rosen (1983) showed that the largest coherences between 40–50-day fluctuations of zonally averaged zonal winds and global momentum were found in tropical latitudes, a result subsequently verified by Benedict and Haney (1988). Lag correlations between zonally averaged momentum and high cloudiness at different latitudes (Risbey and Stone 1988) confirmed the tendency for 40–50-day momentum fluctuations to propagate poleward from near-equatorial latitudes. Corollary evidence of the tropical origin of the global momentum oscillation was provided by studies demonstrating that wind-stress fluctuations in the tropical Pacific could provide the momentum transfer needed to account for the observed conservative momentum exchange between the atmosphere and solid earth (Madden 1987, 1988; Gutzler and Ponte 1990), with forced barotropic ocean modes providing efficient and extremely rapid transfer of momentum from the ocean surface to continental walls (Ponte and Gutzler 1991). Lau et al. (1989) and Gutzler and Ponte (1990) examined in more detail the locations within the tropics that contribute most to momentum variability.

In addition to the tropical manifestations of the 40–50-day oscillation there is increasing evidence of significant extratropical variability on this time scale. Several studies have shown that the extratropical circulation responds to tropical convective variability associated with the 40–50-day oscillation (Weickmann 1983; Lau and Phillips 1986), particularly in the Northern Hemisphere during the winter season. A general overview of extratropical intraseasonal oscillations has been published recently (Ghil and Mo

* The National Center for Atmospheric Research is sponsored by the National Science Foundation.

Corresponding author address: Dr. David S. Gutzler, Aeronomy Laboratory, NOAA/ERL, R/E/AL3, 325 Broadway, Boulder, CO 80303.

1991a,b), showing patterns of intraseasonal variability in both hemispheres. The relationship of these manifestations of 40–50-day variability to the global momentum oscillation is not clear; recently Dickey et al. (1991) have proposed that there may be an oscillation in the extratropical momentum that is essentially separate from the tropical oscillation but interacts with it intermittently.

The intent of the study described in this paper is to extend the observational basis for relating global-scale and local intraseasonal variability by examining seasonal variations of the 40–50-day oscillation in angular momentum for comparison with studies of local seasonality of the tropical 40–50-day oscillation in zonal winds (Madden 1986, hereafter denoted M86; Gutzler and Madden 1989). Our core results are derived from a seasonally varying variance and coherence analysis introduced by M86, which is summarized in the next section. Results of this analysis are presented in section 3. Some of the principal results are verified using a more conventional cross-spectral approach in section 4. A summary and discussion of seasonal variability of the 40–50-day momentum oscillation follow in section 5.

2. Data and analysis technique

We apply the same filtering and spectral analysis techniques developed by M86 to the zonal wind and momentum dataset described by Rosen and Salstein (1983) and Rosen et al. (1987, 1991). Once-daily (0000 UTC) time series of zonal winds for the period 1 January 1976–30 June 1991, analyzed by the U.S. National Meteorological Center onto a 2.5° × 2.5° latitude–longitude grid, are used to create the angular momentum time series. The processing involved in deriving angular momentum from the gridded zonal winds is discussed fully by Rosen et al. (1987, 1991). Briefly, for each day the gridded zonal winds at 10 levels between 1000 and 100 mb are averaged zonally, integrated vertically, and converted to relative angular momentum per latitude unit using the relationship

$$m_\phi = (2\pi a^3/g) \int_{100\text{ mb}}^{1000\text{ mb}} [u]_p \cos^2\phi dp, \qquad (1)$$

where a is the mean radius of the earth, g is gravitational acceleration, $[u]_p$ is the zonally averaged zonal wind at pressure level p, and ϕ is latitude. The daily values of relative angular momentum m_ϕ (which we refer to as simply the momentum) are then interpolated from 2.5° latitudinal strips to 46 equal-area belts of momentum m_b whose unweighted arithmetic sum is the global atmospheric momentum $\mathbf{M}$. For this study we have summed the belt values m_b into three larger near-equal-area regions. Our "tropical" region consists of the 16 belts between latitudes 20.4°S and 20.4°N. The "Southern Hemisphere" (SH) and "Northern Hemisphere" (NH) regions, respectively, comprise the 15 belts poleward of 20.4° in each hemisphere. Thus, the tropical region represents a slightly larger fraction of the total global area ($^{16}/_{46}$ or 34.8%) than either extratropical region ($^{15}/_{46}$ or 32.6% each). We denote the components of $\mathbf{M}$ in the tropics, Northern and Southern hemispheres by $\mathbf{M}_T$, $\mathbf{M}_N$, and $\mathbf{M}_S$, respectively. We also present calculations derived from time series of total extratropical momentum $\mathbf{M}_E$ defined as the sum $\mathbf{M}_N + \mathbf{M}_S$.

In section 3 the time series of $\mathbf{M}$ and its regional components are subjected to bandpass filtering and seasonally varying spectral analysis, as described by M86, who developed the analysis technique to investigate seasonal variations of the 40–50-day oscillation in individual station records in the tropics. The principal filter of interest for this study is the "47-day filter," which has unit response at 47 days and a half-power bandwidth of about 0.010 day^{-1} with half-power response points at periods of approximately 38 days and 61 days. The 47-day filter effectively captures the 40–50-day spectral peak of variance and vertical coherence of zonal winds in the tropical western Pacific. Our use of the 47-day filter in this study facilitates comparison with the local seasonal variability described by M86, but as we will show, it is possible that this filter is not optimally designed for the 40–50-day oscillation in $\mathbf{M}$.

In order to get a more complete picture of the behavior of the low-frequency end of the spectrum, statistics of variability in the 40–50-day period range are compared with similar statistics derived from other intraseasonal frequency bands. First, results derived from two other filters are also shown and discussed. These additional filters have bandwidths equal to the 47-day filter but central (unit response) frequencies shifted ±0.011 day^{-1} to periods of 99 days and 31 days. The amplitude response functions of all three filters are shown in Fig. 4 of M86. Second, in section 4 a description of the frequency dependence of seasonal variability is given by subjecting the momentum time series to conventional cross-spectral analysis.

The time series of momentum are divided into 540-day segments each starting on 1 August of successive years. For example, the segments of $\mathbf{M}$ are filtered to produce time series $\mathbf{M}^{31}$, $\mathbf{M}^{47}$, and $\mathbf{M}^{99}$, where the superscript refers to the central period of the filter. The statistics presented here are derived from 365-day segments of filtered data, with filtered segments starting on 1 October of each year (the filtering process contaminates the endpoints of the 540-day unfiltered segments). Estimates of the seasonally varying variances $S^\tau(t)$ and covariances $C^\tau(t)$ for the three filtered series (τ = 31, 47, and 99) are based on 14-year composites (1976/77–1989/90) averaged over each day t of the year:

$$S^\tau_{\mathbf{M}}(t) = \langle \mathbf{M}^\tau(t)^2 \rangle \qquad (2)$$

$$C^\tau_{\mathbf{M},\mathbf{M}_T}(t) = \langle \mathbf{M}^\tau(t) \cdot \mathbf{M}^\tau_T(t) \rangle, \qquad (3)$$

where the brackets denote an ensemble average over all years for a particular calendar day. Quadrature variances $Q^{\tau}(t)$ corresponding to respective covariances are calculated by shifting one of the filtered time series one-quarter cycle; that is,

$$Q^{\tau}_{\mathbf{M},\mathbf{M}_T}(t) = \langle \mathbf{M}^{\tau}(t) \cdot H(\mathbf{M}_T \tau(t)) \rangle, \quad (4)$$

where H is the Hilbert transform operator. The estimates of $S^{\tau}(t)$, $C^{\tau}(t)$, and $Q^{\tau}(t)$ are also smoothed with a running average equal to τ, the length of the central period of the filter (e.g., a 47-day running average is applied to S^{47}). Seasonally varying estimates of squared coherence $\mathrm{coh}^{\tau}(t)$ and phase $\Phi^{\tau}(t)$ are then derived from the smoothed values of S^{τ}, C^{τ}, and Q^{τ}:

$$\mathrm{coh}^{\tau}_{\mathbf{M},\mathbf{M}_T}(t) = \frac{C^{\tau}_{\mathbf{M},\mathbf{M}_T}(t)^2 + Q^{\tau}_{\mathbf{M},\mathbf{M}_T}(t)^2}{(S^{\tau}_{\mathbf{M}}(t) \cdot S^{\tau}_{\mathbf{M}_T}(t))} \quad (5)$$

$$\Phi^{\tau}_{\mathbf{M},\mathbf{M}_T}(t) = \tan^{-1}(Q^{\tau}_{\mathbf{M},\mathbf{M}_T}(t)/C^{\tau}_{\mathbf{M},\mathbf{M}_T}(t)). \quad (6)$$

A complete description of the digital filters and the seasonally varying spectral estimates is presented by M86.

3. Seasonal variations of intraseasonal momentum fluctuations

Figure 1 shows the 14-year composite of seasonally varying variances $S^{99}_{\mathbf{M}}(t)$, $S^{47}_{\mathbf{M}}(t)$, and $S^{31}_{\mathbf{M}}(t)$, and a fourth variance curve labeled "red," which will be described presently. The variance of **M** decreases with increasing frequency in all months except possibly July and August. Most geophysical time series exhibit decreasing variance with increasing frequency, which can be modeled to a good approximation as a first-order Markov process or "red noise" (Gilman et al. 1963).

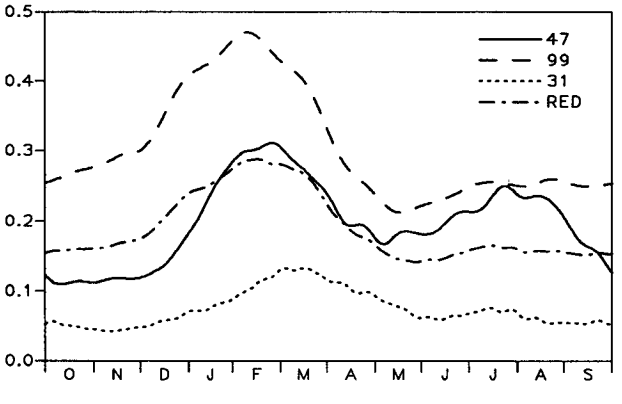

FIG. 1. Spectral estimates as a function of time of year for globally averaged atmospheric angular momentum **M** at $1/99$ day^{-1} (dashed line), at $1/47$ day^{-1} (solid line), and at $1/31$ day^{-1} (dotted line). Estimates are composited over 14 years (1976/77–1989/90). The arithmetic mean of the $1/99$ day^{-1} and $1/31$ day^{-1} estimates, which is the approximate expected value of the $1/47$ day^{-1} estimate based on a red-noise hypothesis, is shown as a dash–dot line. Abscissa is time of year, starting 1 October and ending 30 September; months of the year are delineated on the axis. Ordinate is momentum variance whose units are $(10^{25}$ kg m^2 s$^{-1})^2$.

An absolute spectral peak at the 40–50-day time scale (i.e., a peak standing out from a zeroth-order Markov or "white-noise" null hypothesis, in which the background spectrum is expected to have no frequency dependence) would be indicated by 47-day variances exceeding 99-day (and 31-day) variances. In contrast to time series of upper-tropospheric zonal winds in the western tropical Pacific, for which $S^{47} > S^{99}$ during at least part of the year (M86), such is not the case in the time series of **M**. Previous studies of 40–50-day variability suggest that the spectral peak of angular momentum variance occurs at nearly the same frequency as the near-equatorial 40–50-day oscillation (Rosen and Salstein 1983), but covers a narrower frequency band than the peak in western Pacific wind spectra (Gutzler and Ponte 1990).

A weaker 40–50-day spectral peak than one standing out from a white-noise spectrum would be a peak defined relative to a red-noise background spectrum. As discussed by M86, within the frequency range covered by these filters a red-noise process is reasonably approximated by a linear decrease of variance with increasing frequency. A 40–50-day spectral peak exceeding a red-noise null hypothesis is therefore approximately indicated by 47-day variances exceeding the arithmetic average of the 99-day and 31-day variances. The dash–dot curve in Fig. 1 (labeled "red") plots this average, which is just $(S^{99} + S^{31})/2$. The 40–50-day variance $S^{47}_{\mathbf{M}}$ does exceed this average between January and September, with the most pronounced difference between the 47-day variance and the red variance observed in boreal summer. By this weaker criterion the filters do capture a 40–50-day spectral peak in **M**, and Fig. 1 suggests that the spectral peak first shown by Rosen and Salstein (1983) and Anderson and Rosen (1983) is primarily associated with fluctuations during the boreal winter, spring, and especially summer.

We tried using filters with somewhat narrower passbands in an effort to isolate a clearer signature of a 40–50-day spectral peak but did not achieve results that were substantially superior in this regard to those yielded by the M86 filters. The absence of a more obvious spectral peak makes it difficult for us to interpret our results in terms of any dynamical processes specific to a 40–50-day oscillation. After all, the seasonal variability of $S^{47}_{\mathbf{M}}$ is generally quite similar to the variability of $S^{99}_{\mathbf{M}}$ in Fig. 1, although most of the variability passed by the 99-day filter clearly lies outside the usual frequency range (roughly 30 to 60 days) associated with the 40–50-day oscillation in tropical winds. Figure 1 suggests that the 47-day "peak" in summer may be principally a result of the seasonal depression of lower frequency (99-day) variance rather than a seasonal enhancement of 40–50-day variance. We will examine further the potential sensitivity of our results to the bandwidths of the filters using segment-averaged power spectral analysis in section 4.

The panels in Fig. 2 show the 14-year composite of

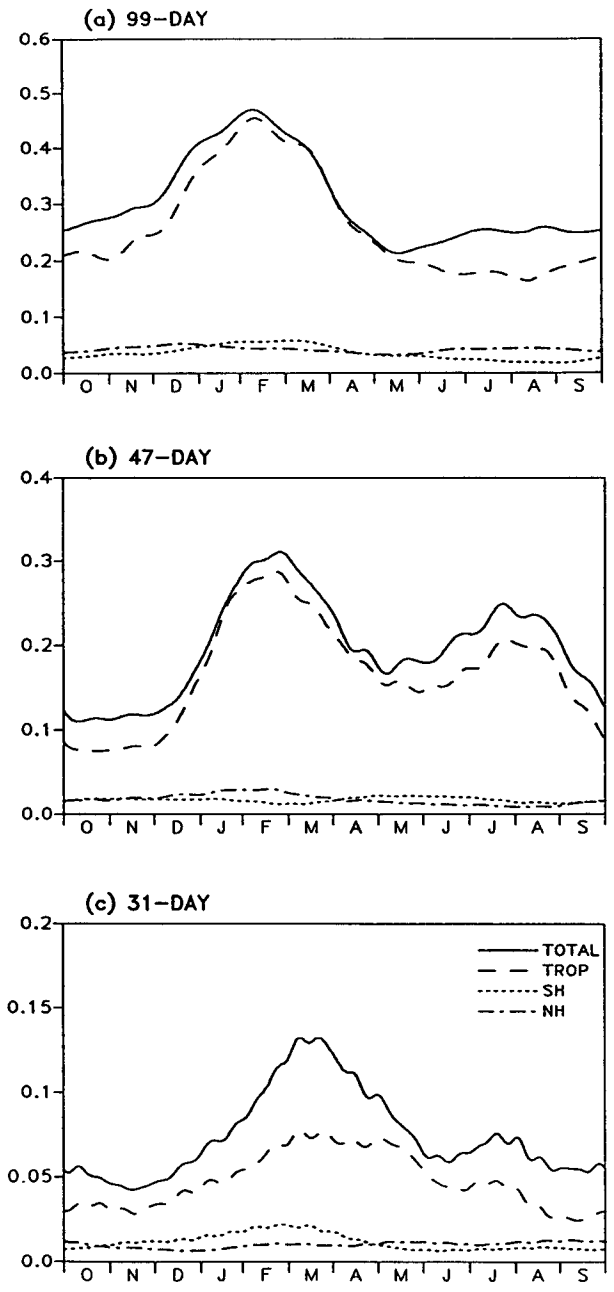

FIG. 2. Spectral estimates as a function of time of year for globally averaged atmospheric angular momentum **M** (solid line) and angular momentum in three near-equal-area latitude zones: within 20.4° of the equator ($\mathbf{M}_T$; dashed line), north of 20.4°N ($\mathbf{M}_N$; dash-dot line), and south of 20.4°S ($\mathbf{M}_S$; dotted line). Units of momentum variance are $(10^{25}$ kg m^2 s$^{-1})^2$. Estimates are composited over 14 years (1976/77–1989/90). (a) 99-day, (b) 47-day, and (c) 31-day filtered data.

seasonally varying $S^{\tau}_{\mathbf{M}}$ for each filter (reproduced from Fig. 1) together with the components of the total angular momentum from the three latitude regions. The preponderance of the variance throughout the year in each intraseasonal frequency band is associated with momentum fluctuations in the tropical region $\mathbf{M}_T$, in accordance with results of Anderson and Rosen (1983) and Benedict and Haney (1988) for 40–50-day fluctuations. A seasonal maximum in late winter–early spring, in both $S_{\mathbf{M}}$ and $S_{\mathbf{M}_T}$, is a ubiquitous feature of intraseasonal momentum variability. Intraseasonal momentum variance in either extratropical hemisphere is very much smaller than the variance of the total or tropical momentum, never exceeding 0.06 variance units $[=(10^{25}$ kg m^2/s$)^2]$. Momentum variances in each hemisphere exhibit a broad and weak seasonal maximum in local winter and minimum in local summer in the 47-day band, but the opposite seasonality is observed in the 99-day and 31-day bands.

The seasonal maximum in $S^{47}_{\mathbf{M}}$ is about 0.3 variance units in February (Fig. 2b). A secondary seasonal maximum of almost 0.25 occurs in July. This feature is much more pronounced in the 47-day statistics than in other frequency bands. Minimum variance, just over 0.1, occurs in October. Thus, the 40–50-day oscillation in **M** undergoes substantial seasonal variability, with the variance in late (boreal) winter exceeding that in early autumn by approximately a factor of 3. This seasonal cycle lags slightly the seasonal cycle of the 40–50-day oscillation found at most of the individual near-equatorial zonal wind records examined by M86, whose characterization of the overall seasonal variability was a winter maximum and summer minimum. The sampling uncertainties associated with the short (14-year) record on which the momentum spectra are based make it difficult to ascertain whether these differences in phase are meaningful.

Figure 3 shows $\mathrm{coh}^{47}(t)$ and $\Phi^{47}(t)$ between **M** and $\mathbf{M}_T$, $\mathbf{M}_N$, $\mathbf{M}_S$, and $\mathbf{M}_E$. The plot in panel (a) confirms the close relationship between **M** and $\mathbf{M}_T$ on 47-day time scales: values of $\mathrm{coh}^{47}_{\mathbf{M},\mathbf{M}_T}$, are high (exceeding 0.6) and phase differences $\Phi^{47}_{\mathbf{M},\mathbf{M}_T}$, are close to zero throughout the year. Maximum values of coherence are obtained during the months when the variances of **M** and $\mathbf{M}_T$ are highest, and minimum values occur in late autumn when variances are low, although the seasonal variability of coherence is not as pronounced as the seasonal variability of the variances of these time series in Fig. 2. The traces of $\mathrm{coh}^{47}_{\mathbf{M},\mathbf{M}_N}$, and $\mathrm{coh}^{47}_{\mathbf{M},\mathbf{M}_S}$ remain at lower values than $\mathrm{coh}^{47}_{\mathbf{M},\mathbf{M}_T}$ throughout the year but show marked seasonal variability: $\mathrm{coh}^{47}_{\mathbf{M},\mathbf{M}_N}$ reaches a maximum of about 0.5 in March, and $\mathrm{coh}^{47}_{\mathbf{M},\mathbf{M}_S}$ has a smaller maximum of 0.3 in late January. The maximum coherence between **M** and $\mathbf{M}_E$ thus also occurs in late boreal winter. Compared to the coherence between **M** and its tropical component, $\mathrm{coh}^{47}_{\mathbf{M},\mathbf{M}_E}$ is smaller, never exceeding 0.5.

The phase difference between 47-day fluctuations of **M** and $\mathbf{M}_N$ in March is almost 90°, indicating a near-quadrature relationship with **M** leading $\mathbf{M}_N$. Fluctuations of **M** also lead those of $\mathbf{M}_S$ at the time of maximum coherence in January, but this phase difference varies seasonally, with $\mathbf{M}_S$ actually leading **M** by about

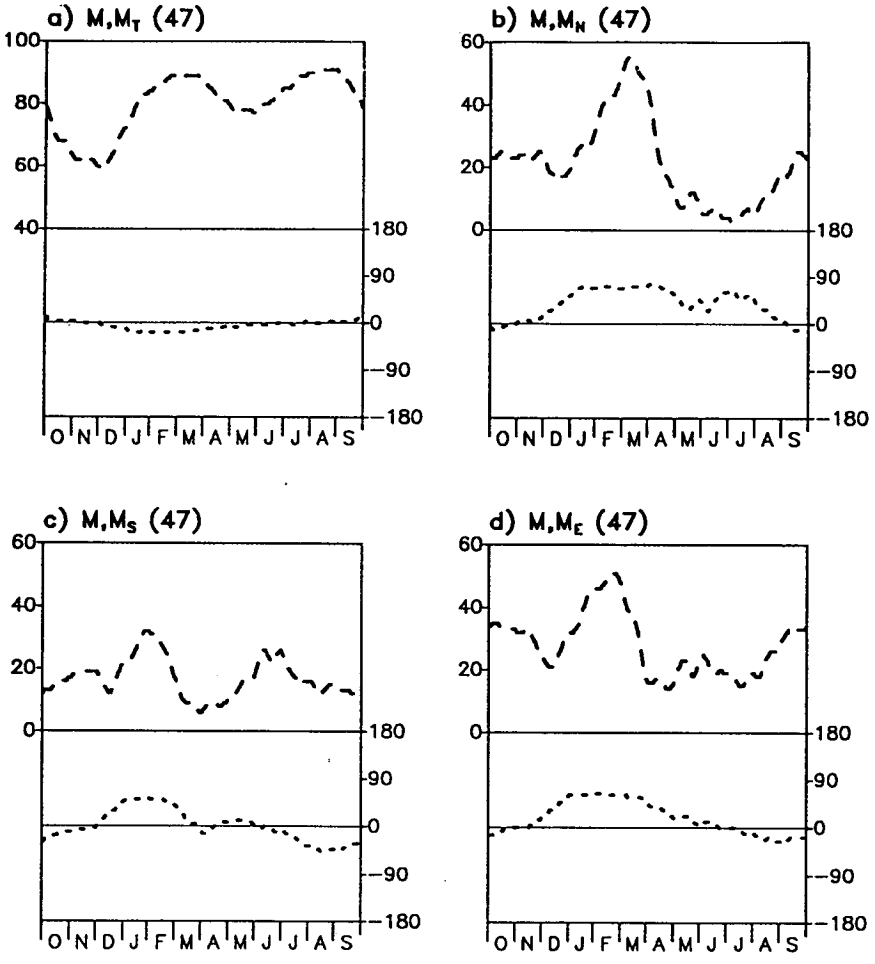

FIG. 3. Squared coherence (dashed line in upper panel) and phase (dotted line in lower panel), as a function of time of year, between 47-day filtered fluctuations of (a) **M** and $\mathbf{M}_T$, (b) **M** and $\mathbf{M}_N$, (c) **M** and $\mathbf{M}_S$, and (d) **M** and $\mathbf{M}_E$, where $\mathbf{M}_E = \mathbf{M}_N + \mathbf{M}_S$. Left-hand ordinate is coh^2 multiplied by 100. Note the different ordinate scale in (a). Positive phase differences indicate that fluctuations in **M** lead those of $\mathbf{M}_T$, $\mathbf{M}_N$, $\mathbf{M}_S$, or $\mathbf{M}_E$. Estimates are composited over 14 years (1976/77–1989/90).

45° during August and September. The global momentum **M** clearly leads the total extratropical momentum $\mathbf{M}_E$ by almost 90° at the time of maximum coherence. At other times of year $\Phi^{47}_{\mathbf{M},\mathbf{M}_E}$ is close to zero, so the extratropics make a small positive contribution to the total momentum **M** (as can be inferred from the observation that $S^{47}_{\mathbf{M}} \sim S^{47}_{\mathbf{M}_T}$ during most of the year).

Figure 4 shows the 47-day coherence and phase between tropical and extratropical components of momentum. The coherence and phase difference between $\mathbf{M}_T$ and $\mathbf{M}_N$ show the late winter maximum and near-quadrature phase difference observed in the corresponding statistics for **M** and $\mathbf{M}_N$ in Fig. 3b. This phase difference, which is consistent with earlier studies documenting propagation of momentum from the tropics into the Northern Hemisphere extratropics (Anderson and Rosen 1983), is clearly indicated in all seasons except the boreal autumn, when $\mathbf{M}_T$ and $\mathbf{M}_N$ fluctuations are not coherent. Values of $\text{coh}^{47}_{\mathbf{M}_T,\mathbf{M}_S}$ are less than 0.3 throughout the year, indicating weaker coupling than is observed between the tropical and NH momentum oscillations. This result is also consistent with the calculation of Anderson and Rosen (1983). The tropical momentum fluctuations lead SH fluctuations (and also total extratropical momentum) during the months of largest coherence in boreal winter.

Momentum fluctuations on the 99-day time scale are also dominated by the tropics: tropical variance greatly exceeds extratropical variance (Fig. 2a), and $\text{coh}^{99}\mathbf{M}$, $\mathbf{M}_T$ (not shown) is between 0.6 and 0.8 throughout the year with no appreciable phase difference. The most obvious qualitative difference between the 99-day statistics and the 47-day statistics concerns the coherence between tropical and extratropical momentum fluctuations. Values of $\text{coh}^{99}_{\mathbf{M}_T,\mathbf{M}_N}$ and

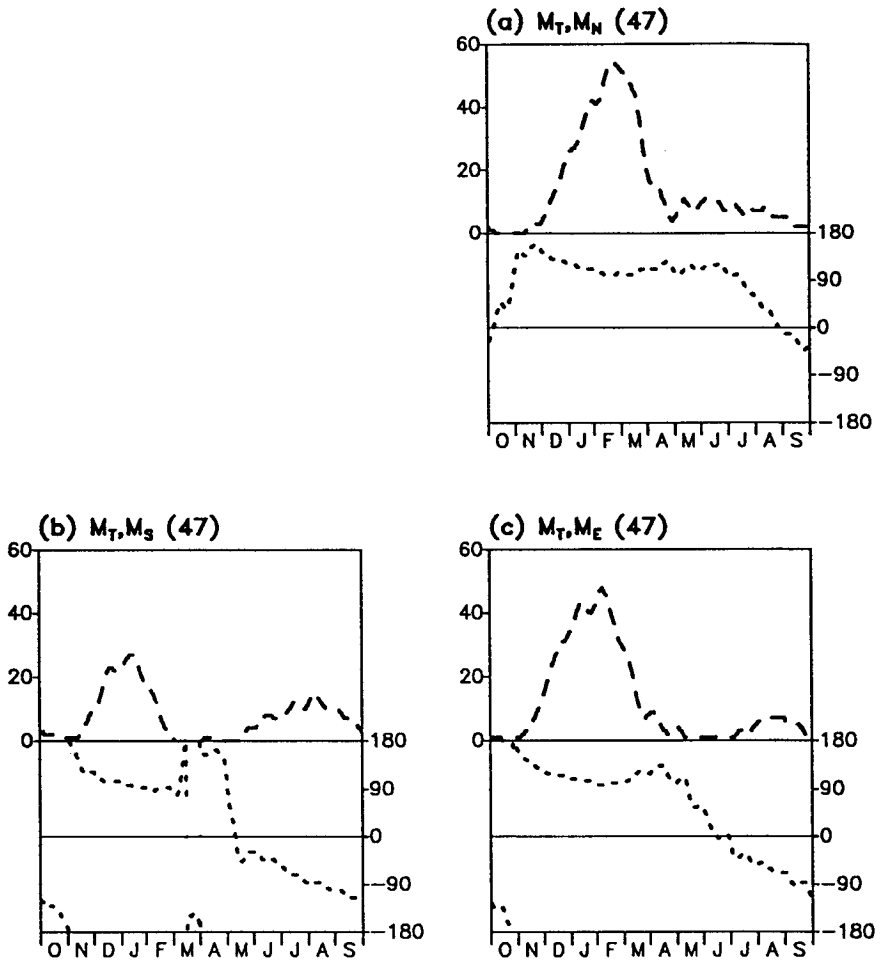

FIG. 4. As in Fig. 3 but for squared coherence and phase between 47-day filtered fluctuations of (a) M_T and M_N, (b) M_T and M_S, and (c) M_T and M_E. Positive phase differences indicate that fluctuations in M_T lead those of M_N, M_S, or M_E. Estimates are composited over 14 years (1976/77–1989/90).

$\text{coh}^{99}_{M_T,M_S}$ (not shown) never exceed 0.25. A signature of coherent tropical–extratropical interaction in boreal winter appears to be the most distinct signature of "special dynamics" on the 40–50-day time scale in these angular momentum calculations.

Sampling uncertainties are a major concern in this study, considering the short temporal length of the time series. The robustness of the principal results described above is tested by calculating independent estimates of seasonally varying variance and coherence derived from the first and second halves (7 years each) of the data record. Figures 5a and 5b show that there are substantial differences between the two halves of the record in the seasonal variability of 47-day variance of M, M_T, M_N, and M_S. The pronounced seasonal maximum in July–August observed in the first composite is entirely absent from the second composite. The February maximum is present in both periods but is considerably weaker in the first period. The dominance of tropical over extratropical momentum variance is apparent in both halves of the record. The July–August peak in the first composite results from a single year (1981), which exhibited very anomalous 40–50-day momentum oscillations in these months. Similarly, the boreal winter of 1988/89 contained very large 40–50-day oscillations that heavily influenced the second half composite. The sensitivity of the composite variances to individual yearly values indicates that sampling uncertainties are large and our results must be interpreted with caution.

Independent 7-year composites of $\text{coh}^{99}_{M_T,M_N}$ are shown in Fig. 6. Both periods exhibit maximum coherence in late boreal winter, but the coherence is much larger in the second half of the 14-year record. The full 14-year composite coherence in February/March (Fig. 4a) is approximately the average of the two 7-year composite values. The near-quadrature phase lag between tropical and Northern Hemisphere momentum

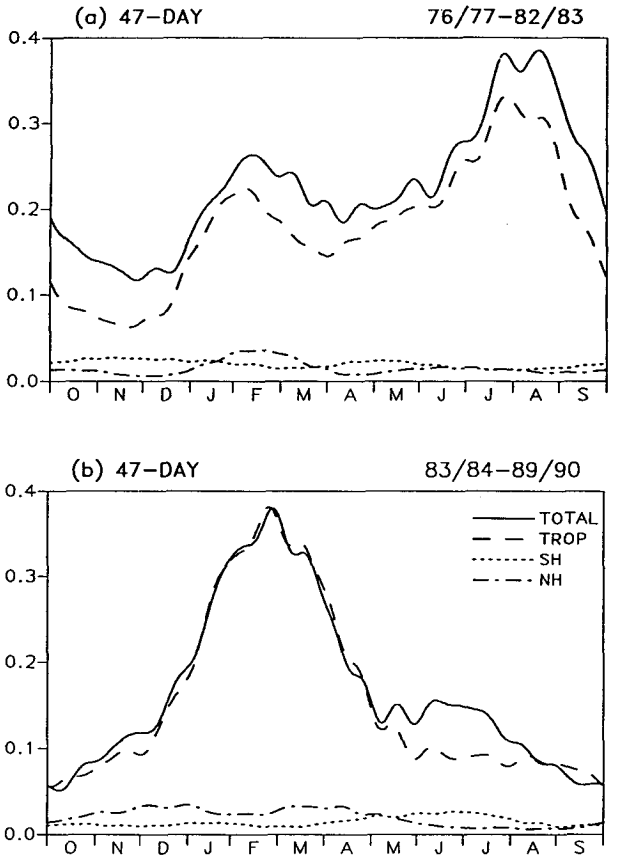

FIG. 5. As in Fig. 2b but derived from the first and second halves (7 years each) of the full data record. (a) Estimates are composited over years 1976/77–1982/83. (b) Estimates are composited over years 1983/84–1989/90.

fluctuations at this time of year is observed in both halves of the record, increasing our confidence in this result. Coherence and phase between M_T and M_S (not shown) are somewhat less reproducible, which is not surprising considering the generally lower level of coherence between these time series.

As a final test of reproducibility, we calculated composite statistics over a 4-year period (1982/83–1985/86) for which we could calculate momentum time series from analyzed winds produced by the European Centre for Medium-Range Weather Forecasts (ECMWF), and compared these results with calculations based on NMC data for the same period. In addition to the different analysis scheme used by the two centers, the ECMWF-based momentum time series included winds at 50 mb. The differences in our composite statistics (not shown) were quite small [consistent with a comparison of other momentum statistics derived from ECMWF and NMC data carried out by Rosen et al. (1987)], indicating that uncertainties in our results due to the particular analysis scheme employed by NMC, and the exclusion of more stratospheric wind data in Eq. (1), are small relative to sampling uncertainty.

4. Segment-averaged spectral analysis of momentum fluctuations

Guided by the seasonal variations identified in section 3, we divide the unfiltered momentum time series

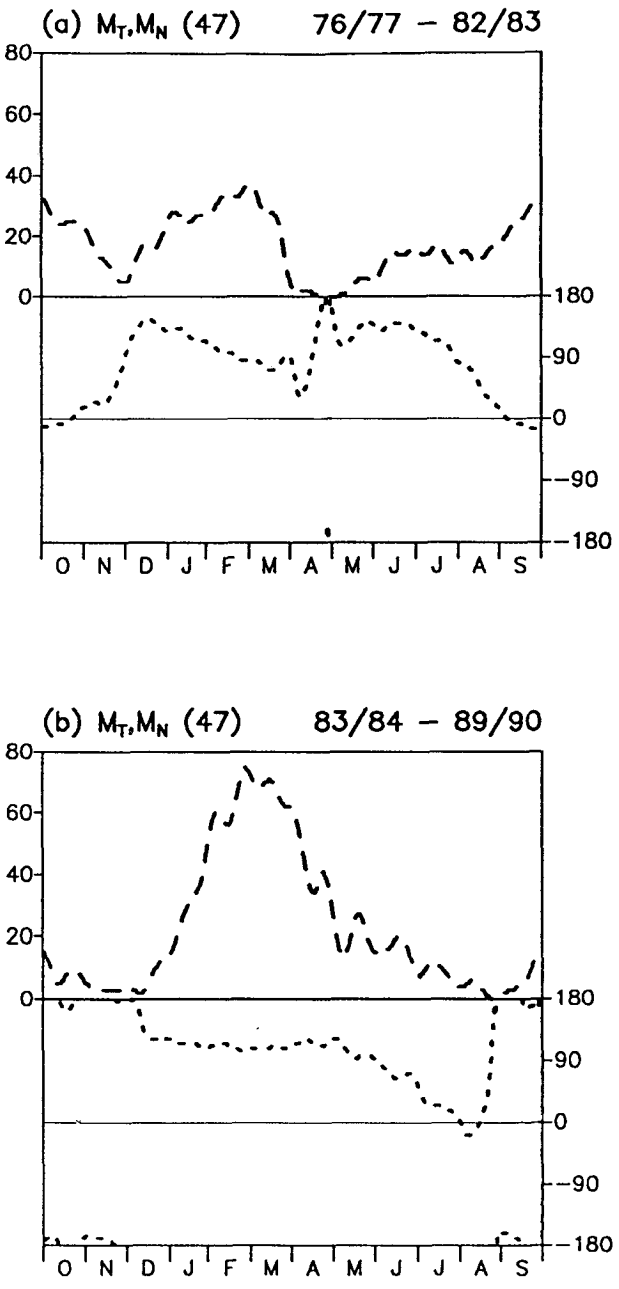

FIG. 6. As in Fig. 4a but derived from the first and second halves (7 years each) of the full data record. (a) Estimates are composited over years 1976/77–1982/83. (b) Estimates are composited over years 1983/84–1989/90.

into 192-day segments (i.e., approximately one-half year) and contrast results of conventional power spectrum and cross-spectrum analysis derived from segments for different halves of the calendar year. The choice of 192 days for the segment length yields spectral lines at periods 96, 48, and 32 days, closely approximating the central response periods of the filtered data. The spectral resolution yielded by the segment-averaged spectra is $1/(192 \text{ days}) \approx 0.0052 \text{ day}^{-1}$, or about half the effective bandwidth of the filters used in section 3. By averaging individual spectral estimates to obtain smoothed spectra (thereby decreasing the spectral resolution) we can examine the sensitivity of the earlier results to the bandwidth of the filters.

Figure 7 shows power spectra of **M** for two different pairs of 192-day segments. In Fig. 7a, we compare the spectra for segments starting 1 November and 1 May. Considering the seasonally varying intraseasonal variance curves in Fig. 1, we expect the spectra to appear red (particularly in the November–April segment), and that the November–April segment will contain more low-frequency variance than the May–October segment. These results are consistent with the power spectra. In fact, dividing the 47-day filtered variance of Fig. 1 by the approximate bandwidth of the filter (0.01 day^{-1}) to obtain the same units shown in Fig. 7 yields an average value over the year of about $20 \times (10^{25} \text{ kg m}^2 \text{ s}^{-1})^2$ day. This value is in good agreement with the spectral estimates at 48-day period in Fig. 7.

Note that there is only the barest hint of a spectral peak at 48-day period in both spectra in Fig. 7a, which may be marginally significant only in the May–October segment. By averaging the spectral estimates over three adjacent lines we obtain the smoothed spectra shown in Fig. 7b, in which any vestige of a 40–50-day spectral peak is obliterated. The 47-day filter has a bandwidth intermediate between the bandwidths of the spectral estimates in Figs. 7a and 7b, so the filter is unable to resolve clearly the rather narrow and weak intraseasonal peak in the **M** spectrum.

It is interesting to compare Fig. 7b with the spectra shown in Fig. B1 of M86. The latter spectra are also calculated by averaging 192-day segments of daily time series and smoothing three adjacent spectral lines, just as in Fig. 7b, but are derived from zonal wind time series at two individual tropical rawinsonde stations.

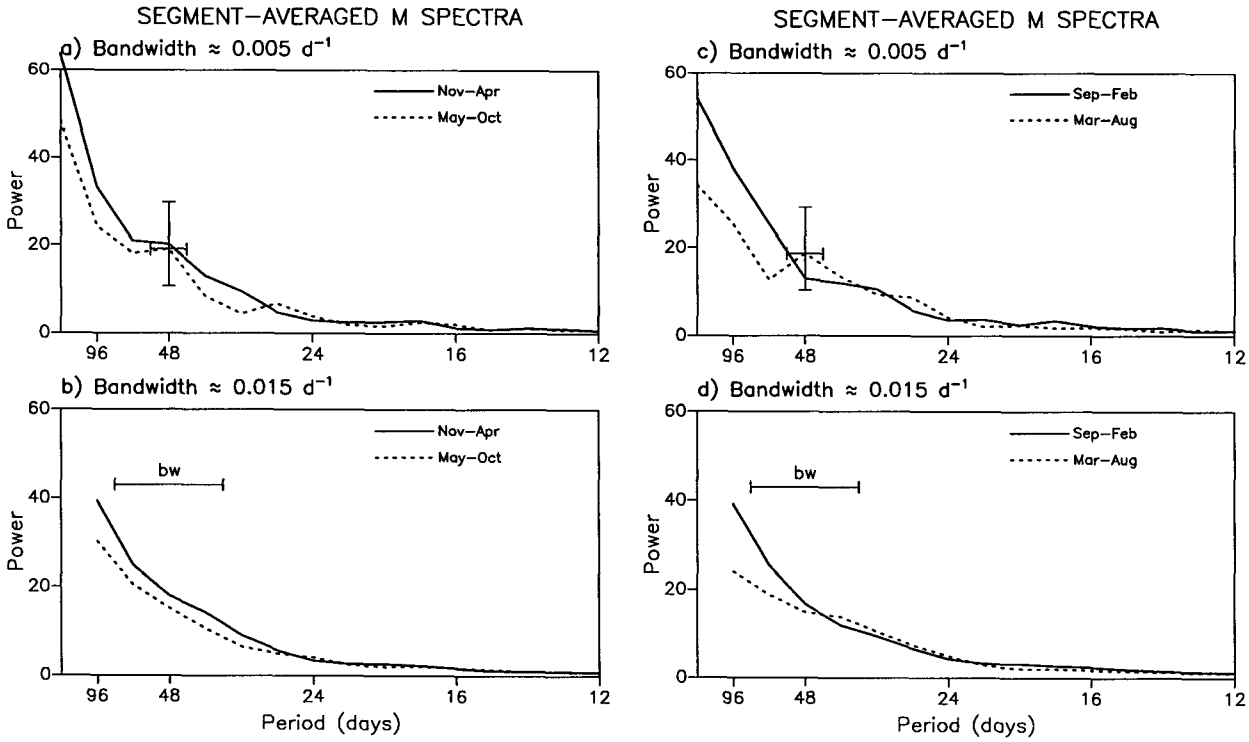

FIG. 7. Segment-averaged power spectral analyses of **M**. In panel (a) the solid line shows the spectral density of **M** (units 10^{25} kg m^2 s^{-1})^2 day) between periods of 192 days and 12 days for an average of 15 192-day segments, each starting on 1 November of successive years; this is denoted the "Nov–Apr segment." The dotted line shows the same quantity for the average of 15 segments starting on 1 May of successive years, the "May–Oct segment." The bandwidth, shown by the horizontal bar centered on the May–Oct 48-day period estimate, is approximately 50% narrower than the bandwidth of the 99-day, 47-day, or 31-day filters. The 95% confidence threshold for the May–Oct 48-day period estimate is also plotted, based on a chi-square test assuming 30 dof (2 per half-year segment). (b) As in (a) but spectral estimates have been averaged over three spectral lines, resulting in smoothed spectra with a bandwidth approximately 50% wider than the filters. (c) As in (a) but derived from different segments. The solid line shows spectral estimates derived from 192-day segments starting on 1 September. The dotted line is derived from segments starting on 1 March. (d) As in (b) but derived from the same segments used for (c).

Their tropical wind spectra exhibit obvious, significant peaks in the 40–50-day band. Thus, the 40–50-day oscillation in tropical zonal winds described by Madden and Julian (1971, 1972) and Madden (1986) seems to be considerably more pronounced and to cover a broader frequency range than the corresponding signal in **M**.

From Fig. 1 we deduced that any 40–50-day spectral peak should be most pronounced in the boreal summer season. We recalculated power spectra of **M** using segments starting on 1 March and 1 September in an attempt to capture a more pronounced spectral peak in the March–August segment. These spectra, shown in Fig. 7c, confirm the presence of an identifiable peak in the March–August segment and the complete absence of a 40–50-day peak in the September–February segment. Nevertheless there is still no evidence for a broadband intraseasonal spectral peak in the smoothed spectra of **M** (Fig. 7d).

The seasonally varying coherence calculations (Figs. 4 and 5) suggested that the coherence between tropical and extratropical momentum fluctuations is quite variable over the course of the year, with relatively large coherence only during boreal winter and spring. Figure 8 contrasts the cross-spectral results between $\mathbf{M}_T$ and $\mathbf{M}_N$ for the November–April and May–October segments. There is a clear, significant peak in coherence between 38 and 48 days in November–April that disappears completely in May–October. The phase difference at the frequencies showing large coherence is roughly 90° ($\mathbf{M}_T$ leading $\mathbf{M}_N$), consistent with the results obtained previously. Another isolated spectral line (at a period of about 14 days) exhibits comparable coherence.

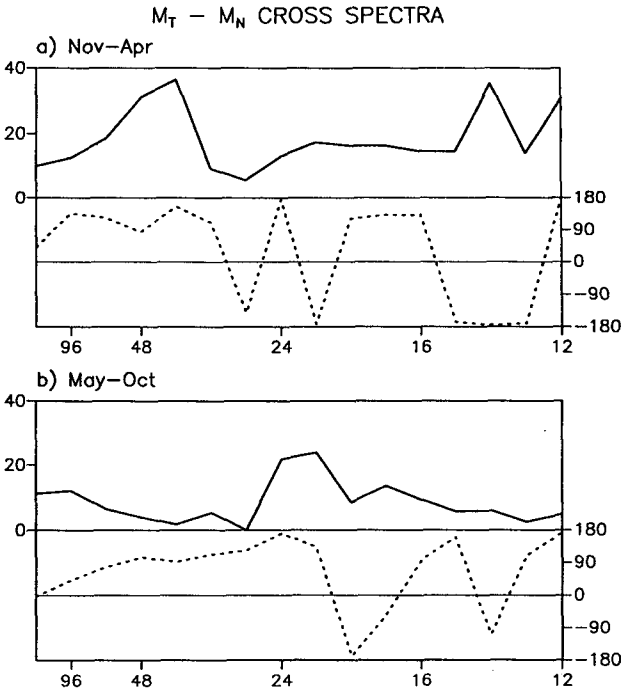

FIG. 8. Coherence and phase between tropical and Northern Hemisphere momentum fluctuations. In the upper half of each panel the solid line shows the squared coherence (multiplied by 100). The a priori 95% significance level for squared coherence at 48-day period is 0.19, assuming 15 degrees of freedom (one per half-yearly segment). The lower half of each panel shows the phase difference in degrees (positive phase implying that $\mathbf{M}_T$ leads $\mathbf{M}_N$). (a) Estimates are derived from the Nov–Apr segment. (b) Estimates are derived from the May–Oct segment.

5. Discussion

The seasonally varying spectra and coherence calculations consistently show that the 40–50-day oscillation in global atmospheric momentum **M** is inherently a tropical phenomenon. Our results extend earlier studies by showing that the variance of momentum at this time scale (in both the tropics and the global average) tends to have largest amplitude in the late (boreal) winter, with a secondary seasonal maximum in summer and relatively depressed variance in spring and autumn. The boreal winter is the season when the oscillation reaches its largest amplitude in individual near-equatorial rawinsonde time series of zonal winds (M86), particularly at stations far from the longitudes of maximum convective variability in the western Pacific (Gutzler and Madden 1989).

We also find, however, that intraseasonal momentum variability in other frequency bands is largest in the winter season, so 40–50-day momentum variability does not stand out from the background spectrum to nearly the same degree exhibited by zonal wind time series at individual tropical locations. The spectral peak in **M** is most pronounced, but still small, in boreal summer, when lower frequency intraseasonal variance is considerably depressed relative to winter variance.

Where within the tropics is the momentum oscillation likely to be most pronounced? First, although the large seasonal cycle of global momentum is principally a manifestation of fluctuations in the strength of the subtropical jet streams (Rosen and Salstein 1983), the low variance found poleward of 20.4° in this study clearly implies that the 40–50-day oscillation in momentum does not result from fluctuations of the jets. Circulation variability equatorward of the jets is required to account for the tropical variability that dominates 40–50-day fluctuations of **M**.

Results from previous studies can be combined to make some inferences about the center of tropical momentum fluctuations. Madden (1987) deduced that 40–50-day fluctuations of **M** reach their maximum value approximately during "phase B" of the canonical 40–50-day oscillation cycle depicted by Madden and Julian (1972), when enhanced convection is weakening over the central Pacific. Studies based on a single boreal summer (Madden 1988) and on eight summers (Kang and Lau 1990) derived the same relationship. From

the same zonally averaged NMC dataset used for this study (but without seasonal stratification), Gutzler and Ponte (1990) determined that the zonally averaged 200-mb zonal wind in belts between 10°–15°S and 15°–20°N latitude vary in phase with M. Lau et al. (1989) showed that positive covariances between local and globally averaged 250-mb zonal wind fluctuations occur at these latitudes in bands extending across South America and the Atlantic Ocean south of the equator, and from Africa to Southeast Asia north of the equator. These longitudes are consistent with the broad region of westerly near-equatorial anomalies characteristic of "phase B" (Madden and Julian 1972). Large, in-phase 47-day filtered zonal wind anomalies in the NH winter season were documented at rawinsonde stations in this longitude band by Gutzler and Madden (1989). The consistent conclusion from these results is that the principal seat of global 40–50-day momentum variations is in tropical but off-equatorial latitudes and is situated well outside the longitudes of maximum 40–50-day tropical convective variability.

This description is similar in several respects to the simulated atmospheric response to prescribed 40–50-day oscillatory equatorial heating described by Anderson and Stevens (1987). Their model produced an off-equatorial upper-tropospheric westerly response and a much smaller equatorial response in quadrature with (lagging) the heating (just as "phase B" lags the maximum near-equatorial convection in the observations). This response was nearly zonally symmetric even though the heating was imposed across just a 90° longitude band on the equator. These features of the response were sensitive to the inclusion of a mean meridional circulation in the model's basic state and the effects of cumulus momentum transport, which respectively enhance and dampen the off-equatorial and equatorial components of the tropical upper-tropospheric response.

One aspect of our observations not accounted for by these (or to our knowledge any other) model results is the seasonal variability of intraseasonal momentum variance. Simplified tropical models of the 40–50-day oscillation are driven either by prescribed latent heating or by prescribed sea surface temperature (which then drives the convective heating). Observations of the seasonal cycles of these variables indicates little or no seasonal variability in the 40–50-day variance of outgoing longwave radiation (Weickmann et al. 1985; Knutson et al. 1986) or in the sea surface temperature of the equatorial Indian and western Pacific oceans (Reynolds 1982). A potential source of tropical momentum is the Northern Hemisphere, which displays a prominent winter seasonal momentum maximum, but our statistics clearly show tropical momentum leading Northern Hemisphere momentum on the 40–50-day time scale in the boreal winter.

Indeed, the momentum in the extratropical atmosphere generally plays a secondary role in our description of global momentum variance. The 40–50-day momentum variance in the Northern Hemisphere (north of 20.4° latitude) is about an order of magnitude smaller than the tropical variance. Seasonal variability of NH momentum can be characterized by an annual cycle with a broad (but weak) maximum from November to March, when the NH and tropical momentum time series are very coherent with the tropics leading the NH by approximately 90°, and smaller variance from May to September. Corresponding 40–50-day fluctuations of Southern Hemisphere momentum are comparably small in magnitude, with the phase of the annual cycle reversed (larger variance in austral winter and smaller in austral summer). Largest coherences between 47-day fluctuations of total momentum and extratropical (NH + SH) momentum are observed in boreal winter with the extratropics lagging total momentum variations by almost one-quarter cycle.

The extratropical 40–50-day variability discussed in the literature tends to be quite wavelike. For example, the patterns of NH winter intraseasonal circulation variability discussed by Weickmann (1983) or Lau and Phillips (1986) have their strongest centers between 30°N and 60°N, but at these extratropical latitudes there are regions of both westerly and easterly anomalies that apparently combine to produce only slight zonally averaged zonal wind anomalies. Furthermore, even large zonal wind anomalies in the extratropics may produce only modest angular momentum anomalies because the surface area and lever arm are small [as described by the $\cos^2\phi$ term in Eq. (1)].

Although extratropical components of 40–50-day momentum variability represent only a small part of the global variability, they may still be related to fluctuations of planetary waves on this time scale (Ghil and Mo 1991a,b). We find 40–50-day momentum fluctuations in the tropics and extratropics to be coherent only in the boreal winter, with the tropical and NH momentum out-of-phase and more coherent than the coupling between tropical and SH momentum fluctuations. These results seem to complement those of Ghil and Mo (1991a,b), who find significant correlation between fluctuations of the leading patterns of intraseasonal variability in the tropics and NH during NH winter and no correlation between tropical and SH intraseasonal modes. Propagation of momentum from tropics to extratropics (roughly characterized in our study in terms of the phase between tropical and extratropical momentum) during boreal winter is a robust feature of the 40–50-day oscillation, and distinguishes 40–50-day variability from other intraseasonal momentum fluctuations.

Acknowledgments. This material is based on work supported by the National Science Foundation under Grant ATM-8819825 (for DSG) and through its sponsorship of the National Center for Atmospheric Research (for RAM and for computing resources). We

thank R. Rosen, D. Salstein, and P. Nelson (AER) for helpful comments and assistance with the NMC wind and momentum time series.

REFERENCES

Anderson, J. R., and R. D. Rosen, 1983: The latitude-height structure of 40–50 day variations in atmospheric angular momentum. *J. Atmos. Sci.*, **40,** 1584–1591.

——, and D. E. Stevens, 1987: The response of the tropical atmosphere to low frequency thermal forcing. *J. Atmos. Sci.*, **44,** 676–686.

Benedict, W. L., and R. L. Haney, 1988: Contribution of tropical winds to subseasonal fluctuations in atmospheric angular momentum and length of day. *J. Geophys. Res.*, **93,** 15 973–15 978.

Dickey, J. O., M. Ghil, and S. L. Marcus, 1991: Extratropical aspects of the 40–50 day oscillation in length-of-day and atmospheric angular momentum. *J. Geophys. Res.*, **96,** 22 643–22 658.

Ghil, M., and K. Mo, 1991a: Intraseasonal oscillations in the global atmosphere. Part I: Northern Hemisphere and tropics. *J. Atmos. Sci.*, **48,** 752–779.

——, and ——, 1991b: Intraseasonal oscillations in the global atmosphere. Part II: Southern Hemisphere. *J. Atmos. Sci.*, **48,** 780–790.

Gilman, D. L., F. J. Fuglister, and J. M. Mitchell, 1963: On the power spectrum of "red noise." *J. Atmos. Sci.*, **20,** 182–184.

Gutzler, D. S., and R. A. Madden, 1989: Seasonal variations in the spatial structure of intraseasonal tropical wind fluctuations. *J. Atmos. Sci.*, **46,** 641–660.

——, and R. M. Ponte, 1990: Exchange of momentum among atmosphere, ocean, and solid earth associated with the Madden-Julian Oscillation. *J. Geophys. Res.*, **95,** 18 679–18 686.

Kang, I.-S., and W. K.-M. Lau, 1990: Evolution of tropical circulation anomalies associated with 30–60 day oscillation of globally averaged angular momentum during northern summer. *J. Meteor. Soc. Japan,* **68,** 237–249.

Knutson, T. R., K. M. Weickmann, and J. E. Kutzbach, 1986: Global-scale intraseasonal oscillations of outgoing longwave radiation and 250 mb zonal wind during Northern Hemisphere summer. *Mon. Wea. Rev.*, **114,** 605–623.

Lau, K. M., and T. Phillips, 1986: Coherent fluctuations of extratropical geopotential height and tropical convection in intraseasonal time scale. *J. Atmos. Sci.*, **43,** 1164–1181.

——, I.-S. Kang, and P. J. Sheu, 1989: Principal modes of intraseasonal variations in atmospheric angular momentum and tropical convection. *J. Geophys. Res.*, **94,** 6319–6332.

Madden, R. A., 1986: Seasonal variations of the 40–50 day oscillation in the tropics. *J. Atmos. Sci.*, **43,** 3138–3158.

——, 1987: Relationships between changes in the length of day and the 40–50 day oscillation in the tropics. *J. Geophys. Res.*, **92,** 8391–8399.

——, 1988: Large intraseasonal variations in wind stress over the tropical Pacific. *J. Geophys. Res.*, **93,** 5333–5340.

——, and P. R. Julian, 1971: Detection of a 40–50 day oscillation in the zonal wind in the tropical Pacific. *J. Atmos. Sci.*, **28,** 702–708.

——, and ——, 1972: Description of global circulation cells in the tropics with a 40–50 day period. *J. Atmos. Sci.*, **29,** 1109–1123.

Ponte, R. M., and D. S. Gutzler, 1991: The Madden-Julian Oscillation and the angular momentum balance in a barotropic ocean model. *J. Geophys. Res.*, **96,** 835–842.

Reynolds, R. W., 1982: A monthly averaged climatology of sea surface temperature. NOAA Tech. Rep. NWS 31, U.S. Department of Commerce. [Available from NOAA/NWS/NMC/Climate Analysis Center, W/NMC52, Washington, DC 20233.]

Risbey, J. S., and P. H. Stone, 1988: Observations of the 30–60 day oscillation in zonal mean atmospheric angular momentum and high cloud cover. *J. Atmos. Sci.*, **45,** 2026–2038.

Rosen, R. D., and D. A. Salstein, 1983: Variations in atmospheric angular momentum on global and regional scales and the length of day. *J. Geophys. Res.*, **88,** 5451–5470.

——, ——, A. J. Miller, and K. Arpe, 1987: Accuracy of atmospheric angular momentum estimates from operational analyses. *Mon. Wea. Rev.*, **115,** 1627–1639.

——, ——, and T. M. Wood, 1991: Zonal contributions to global momentum variations on intraseasonal through interannual time scales. *J. Geophys. Res.*, **96,** 5145–5151.

Weickmann, K. M., 1983: Intraseasonal circulation and outgoing longwave radiation modes during Northern Hemisphere winter. *Mon. Wea. Rev.*, **111,** 1838–1858.

——, G. R. Lussky, and J. E. Kutzbach, 1985: Intraseasonal (30–60 day) fluctuations of outgoing longwave radiation and 250 mb streamfunction during Northern Hemisphere winter. *Mon. Wea. Rev.*, **113,** 941–961.